Chapter 1

Physical and Technical Background

THE fundamental physical phenomenon of magnetic resonance is the existence of nuclear spin. With each spin a magnetic moment is associated making it sensitive to its magnetic environment. In MR(I) a very large ensemble of spins exists. Therefore quantum statistics describes well the behavior of the macroscopic quantities. Whereas the *local* magnetic interactions are responsible for the large amount of available diagnostic information, it is the *external* fields which allow one to retrieve this information and make it observable for the diagnosing physician in modern medical examinations.

This dissertation is based on the development of an external hardware component and therefore the focus of this thesis are interactions with the external magnetic fields and local interactions are ignored unless necessary to understand the discussed imaging behavior. To this end, the spin ensemble is mostly treated as non-interacting. Based on this assumption, the basic equation of motion for the magnetization vector in an external magnetic field is derived. This equation is purely classical and therefore the further physical treatment can be performed with classical electromagnetic theory. To produce image contrast, relaxation effects are exploited, which are the result of spins interacting with their magnetic neighborhood. At some places in this thesis, these effects are considered by extending the equation of motion for the magnetization to the famous Bloch equations.

MRI signals are created by first magnetizing the object under examination with a constant, strong magnetic field, then perturbing the equilibrium magnetization with a transverse RF field before encoding the object with magnetic gradient fields and finally receiving the signal with RF-receiver coils. The frequency and phase content of the received signals strongly depends on the geometric and temporal characteristics of the magnetic fields involved. This implies that a very high standard of coil design and electronic integration is required for high-quality spectra or images in MR(I), one reason among others, which make MR(I) an extremely powerful, but also challenging technology.

G. Schultz, *Magnetic Resonance Imaging with Nonlinear Gradient Fields,*
DOI 10.1007/978-3-658-01134-5_1, © Springer Fachmedien Wiesbaden 2013

The basic physical principles of MR(I) are well understood. Far from being complete, only the most important results are reviewed here. For a detailed physical treatment of the magnetic resonance phenomenon consult [95]. Similarly, only the basic technical features of those hardware components are presented, which are used to generate the required external magnetic fields. A thorough description of the technical realization of an MR scanner is presented in chapter 15.1 of [123], page 540 - 598. Considering that within the PatLoc project a different kind of encoding hardware has been developed, special emphasis is placed on the gradient system and its main purpose: signal localization. In PatLoc, signal localization with a modified gradient hardware is not sufficient in general and should therefore be accompanied with parallel image acquisition; this topic is therefore also touched at the end of this chapter.

1.1 Nuclear Magnetic Resonance

In this section, the physical principles of MR are presented and the basic NMR experiment, fundamental to MR spectroscopy and MR imaging, is analyzed involving

- magnetization of the object under examination with the main magnet,
- excitation of the magnetization with an RF-transmit pulse and
- signal reception with the RF-receiver unit.

1.1.1 Physical Principles

The physics of MR is based on the physics of the nuclear spin. The spin is a non-classical property and therefore quantum mechanics is the correct framework for describing its dynamics. The basic observation is that a spin can be regarded as an intrinsic angular momentum of the nucleus. A nucleus consists of charged particles and therefore with the spin a magnetic moment $\hat{\mu}$[1] is associated, which points along the direction of the spin angular momentum $\hat{S}$:

$$\hat{\mu} = \gamma \hat{S}. \tag{1.1}$$

[1] The hat indicates quantum mechanical operators.

The proportionality constant γ is termed *gyromagnetic ratio*. This ratio is different for each nucleus. For the most important nucleus in MR, hydrogen, with spin $1/2$, it has the value $\gamma = 267.52\ 10^6\,{}^{\mathrm{rad}}/_{\mathrm{Ts}}$, also denoted as $\gamma = \gamma/(2\pi) = 42.58\,{}^{\mathrm{MHz}}/_{\mathrm{T}}$.

Having a magnetic moment, the spin interacts with the magnetic field $\vec{B}$ at its location. The interaction energy is described by the Hamiltonian:

$$\hat{H} = -\hat{\mu}\vec{B}. \tag{1.2}$$

In the NMR experiment, a macroscopic voltage is measured in the receiver chain. The voltage is induced by the magnetization of the measured object, which can itself be regarded as a macroscopic (spatially-dependent) property. Quantum statistics can be used to bridge the gap between microscopic quantum theory and macroscopic measurements. In NMR, quantum statistics gives very accurate results because the (local) sample sizes involve around 10^{22} spins.

These large spin ensembles exhibit a macroscopic magnetization under the influence of external magnetic fields. But what is the exact effect of those fields onto the magnetization?

To answer this question, a non-interacting spin ensemble is assumed, which is a very good assumption within the scope of this thesis. The relevant findings can be deduced based on the density operator formalism. The density operator is defined as $\hat{\sigma} := \overline{|\psi\rangle\langle\psi|}$, where the overbar indicates averaging over all independent sample quantum states.

The (macroscopic) magnetization density $\vec{M}$ at location $\vec{x}$ and time t is then found by calculating

$$\vec{M}(\vec{x},t) = n(\vec{x}) \cdot < \hat{\mu} >= n(\vec{x}) \cdot Tr\left\{\hat{\sigma}(\vec{x},t)\hat{\mu}\right\}, \tag{1.3}$$

where $n(\vec{x})$ is the spin density. The dynamics of the magnetization is therefore entirely defined by the dynamics of the density operator. The time evolution of this operator is described by the von Neumann equation:

$$\frac{\mathrm{d}\hat{\sigma}}{\mathrm{d}t} = -\frac{\mathrm{i}}{\hbar}[\hat{H},\hat{\sigma}]. \tag{1.4}$$

In this equation, $\hbar$ denotes the reduced Planck constant, which has a value of 1.05×10^{-34} Js. The time derivative of the individual components of the magnetization is found by combining Eqs. 1.2 - 1.4:

$$\frac{\dot{M}_i}{n} = \frac{\mathrm{d}}{\mathrm{d}t} Tr\left\{\hat{\sigma}\hat{\mu}_i\right\} = -\frac{\mathrm{i}}{\hbar} Tr\left\{[\hat{H},\hat{\sigma}]\hat{\mu}_i\right\} = +\frac{\mathrm{i}}{\hbar}\sum_j Tr\left\{\hat{\sigma}[\hat{\mu}_i,\hat{\mu}_j]B_j\right\}.$$

According to Eq. 1.1, the commutator relations of the magnetization operator follow the common relations of the spin angular momenta:

$$[\hat{\mu}_i,\hat{\mu}_j] = \gamma^2[\hat{S}_i,\hat{S}_j] = \mathrm{i}\hbar\gamma^2\sum_k \epsilon_{ijk}\hat{S}_k = \mathrm{i}\hbar\gamma\sum_k \epsilon_{ijk}\hat{\mu}_k,$$

where ϵ_{ijk} is the Levi-Civita symbol. The time derivative of M_i is therefore found to be:

$$\dot{M}_i = -n\sum_{j,k}\epsilon_{ijk} Tr\left\{\hat{\sigma}\hat{\mu}_k\right\}(\gamma B_j) = -\sum_{j,k}\epsilon_{ijk} M_k(\gamma B_j) = (\vec{M}\times(\gamma\vec{B}))_i,$$

and the dynamics of the magnetization vector is described with a simple equation:

$$\dot{\vec{M}} = \vec{M}\times(\gamma\vec{B}). \tag{1.5}$$

This equation is the macroscopic equation of motion of the magnetization vector. This equation is also known from classical physics. Most results in this thesis are based on this classical equation, and therefore mostly a quantum mechanical treatment can be omitted and established techniques from classical electrodynamics are employed instead.

1.1.2 Main Magnetic Field

Starting from an initial state, the equation of motion presented in Eq. 1.5 can be integrated for known magnetic fields. However, the initial state requires at least some magnetization. The most important purpose of the main magnetic field $B_0\vec{e}_z$ is to polarize the object under examination.

Figure 1.1: This MR scanner (MAGNETOM Trio, A Tim System 3T, Siemens Healthcare, Erlangen, Germany) was equipped with a PatLoc insert coil while this thesis was conducted. The scanner is shown during delivery to the site of installation. Visible from outside is the vacuum chamber that contains the main magnet, the largest component of the scanner.

a) Main Magnet

The magnetic field is generated with the large main magnet (cf. Fig. 1.1). The field strength determines the precession frequencies of the magnetization. A major engineering criterion is spatio-temporal homogeneity of the precession frequencies. Therefore, the magnet design is based on a superconducting solenoid which generates very homogeneous fields with an accuracy of around $0.1 - 10ppm$ in the typical imaging region. Typical field strengths for imaging patients range from $0.2\,\mathrm{T} - 3\,\mathrm{T}$. An $11.75\,\mathrm{T}$ system (Iseult/INUMAC project) is planned to be delivered in April 2013 to the Neurospin site in Saclay, France [187]. It will be largest and strongest whole-body system ever built. Experimental or pre-clinical scanners often have even stronger fields of up to $20\,\mathrm{T}$. One advantage of such strong systems is an increase in SNR. Most clinical magnets are shielded with a second superconducting coil. The shield reduces efficiency in favor of enhanced patient safety and siting costs resulting from fast decaying magnetic fields outside of the examination area.

b) Polarization

With the main magnet, the measured object is polarized. But how does the generated constant magnetic field $B_0\vec{e}_z$ actually create the nuclear mag-

netization in the sample? In order to find a reliable value of the initial magnetization methods from quantum statistics should be used. The initial magnetization is established in the thermodynamic equilibrium. In this equilibrated state, the off-diagonal elements (coherences) of the density operator are zero. The diagonal elements (populations) are weighted according to their corresponding Boltzmann factors:

$$\sigma_{mm}^{eq} = \frac{1}{Z} exp(^{-E(m)}/_{k_B T}). \tag{1.6}$$

The value $Z = \sum_m exp(-E(m)/k_B T)$ represents the canonical partition function, k_B is the Boltzmann constant with value $k_B = 1.38 \times 10^{-23} JK^{-1}$, T is the temperature and $E(m)$ is the energy of the corresponding Zeeman quantum state. For a constant field $B_0 \vec{e}_z$ the energy levels $E(m)$ are, according to Eqs. 1.1, 1.2, given by:

$$E(m) = m\hbar\gamma B_0,$$

where m is the quantum number of the z-angular momentum $\hat{S}_z$. In NMR, the Boltzmann factor $B = {}^{\hbar\gamma B_0}/_{k_B T}$ is typically only about 10^{-5}. Therefore, the exponentials in Eq. 1.6 can be simplified using a Taylor series expansion and for a spin $1/2$ system with only two Zeeman states ($m = \pm 1/2$) the equilibrium density operator reduces to:

$$\hat{\sigma}^{eq} = \begin{pmatrix} \frac{1}{2} + \frac{1}{4}B & 0 \\ 0 & \frac{1}{2} - \frac{1}{4}B \end{pmatrix}.$$

The initial magnetization $\vec{M}^{eq}$ is then found with the relations presented in Eqs. 1.1, 1.3:

$$\begin{aligned} M_x^{eq} &= M_y^{eq} = 0, \\ M_z^{eq} &= n \cdot \gamma \cdot Tr\left\{\hat{\sigma}^{eq}\hat{S}_z\right\} = \frac{1}{4}\frac{\hbar^2\gamma^2}{k_B T} n B_0 \overset{B_0 = 1.5\,\mathrm{T}}{\approx} 5 \times 10^{-3}\,{}^{\mathrm{J}}/_{\mathrm{Tm}^3} \\ &\approx 4 \times 10^{-9} B_0/\mu_0, \;\; \mu_0 = 4\pi \cdot 10^{-7}\,{}^{\mathrm{Tm}}/_{\mathrm{A}}. \end{aligned} \tag{1.7}$$

The resulting nuclear paramagnetism of water has a susceptibility of only 4×10^{-9}. It is about 2000 times weaker than the actual diamagnetism of water. The contribution of the nuclear spins to the longitudinal magnetization is therefore negligible. Nevertheless, it is strong enough to be detected once being moved out of equilibrium as shown below.

c) Precession

In the thermodynamic equilibrium, $\vec{M}^{eq}$ does not change in magnitude and direction. If the thermodynamic equilibrium is disturbed, a magnetization vector $\vec{M}_0$ might result with non-zero transverse components. For a constant magnetic field $B_0\vec{e}_z$ the equation of motion, given by Eq. 1.5, can be solved analytically. With an initial magnetization $\vec{M}_0$ the solution is simply:

$$\vec{M}(t) = \mathbf{R}(\vec{e}_z, \omega_L t)\vec{M}_0.$$

The matrix $\mathbf{R}$ is just a standard 3D rotation matrix that describes a rotation by the angle $\omega_L t$ around the z-axis (cf. definition of $\mathbf{R}(\cdot,\cdot)$ in Appendix A.1 on page 291). As the angle increases linearly with time, the motion of the magnetization is indeed a precessional motion around the z-axis (cf. Fig. 1.2) with the *Larmor frequency* ω_L:

$$\omega_L = -\gamma B_0. \tag{1.8}$$

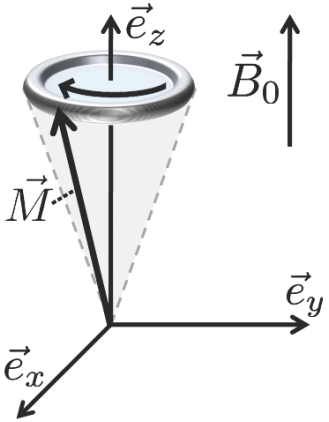

Figure 1.2: Precession of the magnetization vector around the direction of the static main magnetic field.

d) Relaxation and the Bloch Equations

For the assumed non-interacting spin ensemble, the precessional motion goes on forever. In reality, however, the spins interact with each other and their charged neighborhoods. The magnetization therefore slowly relaxes toward its equilibrium value $\vec{M}^{eq}$. The longitudinal relaxation gives rise to the diagnostically very important T_1-contrast and the transverse relaxation to the T_2-contrast. This macroscopic relaxation effect is described by the Bloch equations [11], which modifies the basic equation of motion presented in Eq. 1.5:

$$\dot{\vec{M}} = \vec{M} \times (\gamma \vec{B}) - T_2^{-1} \left(M_x \vec{e}_x + M_y \vec{e}_y\right) - T_1^{-1}(M_z - M_z^{eq})\vec{e}_z. \qquad (1.9)$$

There are many other interaction effects, like for example chemical shift or diffusion, which can correctly be treated with an appropriate model. These effects give rise to a modification of the above Bloch equations [182]. Within the scope of this thesis, these effects are, however, irrelevant and therefore they are ignored.

e) Rotating Frame Formalism

Consider a reference frame, which rotates with $\vec{\omega}$ compared to the laboratory frame. If ∂_t^{rot} describes the time derivative in the rotating frame, the equation of motion (Eq. 1.5) takes the following form:

$$\partial_t^{rot} \vec{M} = \vec{M} \times (\gamma \vec{B} + \vec{\omega}). \qquad (1.10)$$

For a reference frame which follows exactly the precessional motion of the magnetization, i.e., $\vec{\omega} = \omega_L \vec{e}_z = -\gamma B_0 \vec{e}_z$, the effect of the constant main magnetic field $\vec{B} = B_0 \vec{e}_z$ is formally eliminated: Equation 1.10 reduces to $\partial_t^{rot} \vec{M} = 0$; the magnetization vector in the rotating reference frame is therefore fixed in time.

1.1.3 RF Excitation

The RF-transmit system serves to "excite" the magnetization by moving it out of thermodynamic equilibrium. RF excitation is essential

- because the static longitudinal magnetization is very weak and cannot be measured effectively. It is the dynamic motion in the transverse plane, which induces measurable currents in the RF-receiver coils.
- because the return of the magnetization back to thermodynamic equilibrium is tissue-dependent and provides image contrasts with a high relevance for medical diagnostics.

a) RF-Transmit System

The object is excited by irradiating appropriate RF pulses into this object. Fig. 1.3 schematically shows the hardware typically involved in the signal transmission process and the caption explains the purpose of the individual components of the transmit chain.

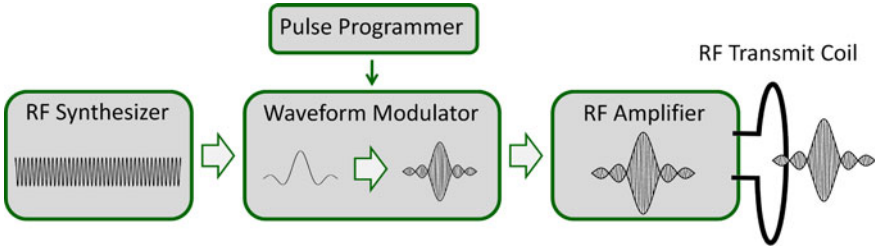

Figure 1.3: Typical RF-transmit chain. An RF synthesizer generates a continuous waveform typically oscillating at the Larmor frequency, from which pieces of the desired pulse duration are cut. A waveform modulator adjusts the pulse in amplitude and phase according to the digital instructions of the sequence programmer and sends it to the RF-power amplifier. Finally, the amplified pulse is coupled to the RF-transmit coil, which irradiates the RF field into the object under examination.

b) Excitation

Consider on-resonance excitation with a transmitting RF field $\vec{B}_1(t)$. On-resonance means that the field rotates with the Larmor frequency, given by Eq. 1.8, in the direction of the rotating reference frame. Even if the transmit field has a longitudinal component along the z-axis or an opposing rotational component, it is sufficient to only consider the rotation along the rotating Larmor frame as those other components have a negligible impact on the dynamics of the magnetization under normal imaging conditions (cf. note 7 of chapter 8 in [95]). The transmit field can therefore be assumed to

be directed in the transverse plane. With an initial direction along the x-axis it is given by:

$$\vec{B}_1(t) = B_1(t)(\cos(\omega_L t)\vec{e}_x + \sin(\omega_L t)\vec{e}_y) = B_1(t)\mathbf{R}(\vec{e}_z, \omega_L t)\vec{e}_x = B_1(t)\vec{e}'_x.$$

The vector $\vec{e}'_x$ describes the fixed x'-axis in the rotating reference frame and the vector $\vec{e}_x$ describes the fixed x-axis in the laboratory frame. The latter equality holds because the two vectors $\vec{e}'_x$ and $\vec{e}_x$ are linked via $\vec{e}'_x = \mathbf{R}(\vec{e}_z, \omega_L t)\vec{e}_x$. In the rotating reference frame, the transmit field therefore points along the $\vec{e}'_x$-direction. The magnetic field envelope $B_1(t)$ might have a time-dependency, which is assumed to be slowly varying compared to the Larmor frequency. When the transmit field is added to the main magnetic field, the equation of motion (Eq. 1.10) reduces to:

$$\partial_t^{rot}\vec{M} = \gamma B_1(t)(\vec{M} \times \vec{e}'_x).$$

The dynamics described by this equation is just a precessional motion around the x'-axis with the *Rabi frequency* $|\omega_R| = \gamma B_1$. If the on-resonance transmit field is switched on for a duration τ, the magnetization is therefore flipped away from the z'-axis around the x'-axis by the flip angle α given by:

$$\alpha = \gamma \int_{t=0}^{\tau} B_1(t)\,\mathrm{d}t. \tag{1.11}$$

This flip affects the magnetization vector accordingly:

$$\begin{aligned}\vec{M}(\alpha, t) &= M_z^{eq}\left(\cos(\alpha)\vec{e}'_z + \sin(\alpha)\vec{e}'_y\right) \\ &= M_z^{eq}\left(\cos(\alpha)\vec{e}_z + \sin(\alpha)\mathbf{R}(\vec{e}_z, \omega_L t)\vec{e}_y\right).\end{aligned} \tag{1.12}$$

The same applies to any initial magnetization $\vec{M}_0$ other than the equilibrium magnetization. The resulting flip of the magnetization vector is the physical interpretation of what is normally referred to as "excitation". Off-resonance excitations, where the transmit field rotates with a slightly different frequency than the Larmor frequency, lead to more complicated motions of the magnetization vector. The dynamics are, however, fully described by the Bloch equations. Closed-form solutions to these equations exist only under special imaging conditions (an example is discussed in section 1.2.3,

page 32ff). In general, the dynamics of the magnetization vector is found by numerical integration.[2]

1.1.4 NMR Signal Detection

The final step in acquiring an NMR signal is to detect the excited magnetization. This is done with receiver coils which are sensitive to the fast magnetic field variations caused by the precessing magnetization.

a) RF-Detection System

A typical RF-detection system is schematically depicted in Fig. 1.4 and explained in detail in the caption. Consult the textbook [111] for a detailed presentation of RF coil and circuit design.

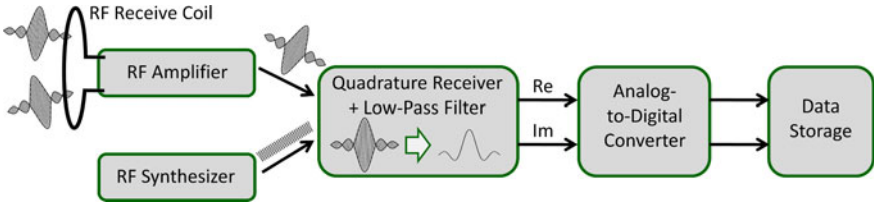

Figure 1.4: Typical RF-receiver chain. First, the signal is received with one or more receiver coil probeheads. The small signals are amplified before being sent to the quadrature receiver. In this hardware component, the signals are multiplied with sinusoidal waveforms from an RF synthesizer having a reference carrier frequency of the same frequency as used for signal transmission. There are two reference signals, shifted by $90\,^{\circ}$. The outgoing signals form, after low-pass filtering and digitization in an analog-to-digital converter (ADC), real and imaginary part of the NMR signal, which is finally stored using appropriate hardware.

b) Free Induction Decay

The influence of the individual components of the RF-detection system onto the NMR signal can also be quantified, which is the topic of this section.

First, consider that the precessing magnetization generates a magnetic field which is induced in an RF-receiver coil. Based on Faraday's law of induction

[2] Nice animations of spin dynamics can found at [150].

and a reciprocity law [68][3], it can be shown that the induced voltage U in the receiver coil is given by:

$$U(t) = -\dot{\Phi}(t) = -\frac{\mathrm{d}}{\mathrm{d}t}\int_V \vec{\mathfrak{B}}^{re}(\vec{x})\vec{M}(\vec{x},t)\,\mathrm{d}\vec{x}. \tag{1.13}$$

Here, Φ is the magnetic flux through the receiver coil, V is the excited volume and $\vec{\mathfrak{B}}^{re}$ is the magnetic field generated by the receiver coil per unit current.[4] The time derivative of M_z can be neglected because the precessional motion is restricted to the xy-plane. Therefore, introduction of Eq. 1.12 into the above equation leads to a voltage of:

$$U(t) = \omega_L \int_V M_z^{eq}(\vec{x})\sin(\alpha)\left(\mathfrak{B}_x^{re}(\vec{x})\cos(\omega_L t) - \mathfrak{B}_y^{re}(\vec{x})\cos(\omega_L t + \frac{\pi}{2})\right)\mathrm{d}\vec{x}. \tag{1.14}$$

The signal is amplified by a factor β_A, it is split in two and modulated in the quadrature receiver. The effect of the quadrature receiver can be explained with a multiplication of the signal, represented by Eq. 1.14, with a sinusoid tuned at the transmit frequency. The output therefore consists of two signals s_1 and s_2, where s_1 has been multiplied with $2\cos(\omega_L t)$ and s_2 has been multiplied with the phase-shifted reference signal $2\cos(\omega_L t + \pi/2)$. After a low pass filter, the two signals are formally combined to form a complex signal $s(t)$:

$$s(t) = s_1(t) + \mathrm{i}s_2(t) = \int_V m(\vec{x})c(\vec{x})\,\mathrm{d}\vec{x}, \tag{1.15}$$

$$\begin{aligned} m(\vec{x}) &:= \omega_L \beta_A M_z^{eq}(\vec{x})\sin(\alpha), \\ c(\vec{x}) &:= \mathfrak{B}_x^{re}(\vec{x}) - \mathrm{i}\mathfrak{B}_y^{re}(\vec{x}). \end{aligned} \tag{1.16}$$

The quantity $c(\cdot)$ is usually termed *RF-coil sensitivity*. *Spin density* is a common term to denote the quantity $m(\cdot)$. This definition is problematic,

[3]The used model is valid for field strengths of up to about $1.5\,\mathrm{T}$ on whole-body systems. The model assumes that the magnetic field generated by the excited magnetization has an immediate effect on the magnetic flux in the receiver coil (near-field). For higher field strengths however, time lags must be considered [67]. Consult for example [66] for a correct treatment beyond the near field or Appendix E in [163], where a formula for the induced voltage is presented.

[4]Here, too, the limited validity of Eq. 1.13 becomes apparent. The derivation of Eq. 1.13 models the receiver coil as a simple wire loop and not as a resonant structure, as it should correctly be done [163]. It is assumed that the coil's DC sensitivity equals its RF sensitivity. Interactions with the measured object are ignored. In practice the RF sensitivity depends on the electromagnetic properties of the object and the frequency (also cf. [201]), and therefore the RF sensitivity is typically determined for each scan separately (also cf. chapter 2.1.2b, page 48).

but might be justified because, according Eqs. 1.7, 1.16, m is actually proportional to the spin density. However, small deviations occur when the transmit field is not homogeneous because, in this case, the flip angle is not constant over the entire excitation volume (cf. Eq. 1.11). Though not exact as well, it is also common to denote $m(\cdot)$ as *magnetization*. In this thesis both terms, *spin density* and *magnetization*, are used to describe $m(\cdot)$. In the following, the dependency of m on the amplification β_A will be suppressed by assuming w. l. o. g. $\beta_A := 1$.

The signal presented in Eq. 1.15 is the measured signal of the NMR experiment. This signal is constant because relaxation effects have been ignored in these calculations. In reality the presence of transverse relaxation causes the signals to decay. This decaying signal is called the *free induction decay*, or in short, the *FID*.

c) Signal-to-Noise Ratio

Physical measurements are always of a statistical nature. The main sources of noise for MRI are thermal motions of charged particles. It is obvious that the electrons in the receiver electronics add to the resulting noise. However, in NMR, it is the charged ions of the objects under examination, which typically form the dominant part of the resulting noise. Whereas elaborate designs of the receiver electronics can lead to a significantly reduced noise contribution, thermal motion of the ions of the measured object cannot be influenced by the experimenter. Noise in the electronic devices might pose a problem with micro-architectures [55]. However, in this work, micro-coils were not used and therefore the discussion of noise is uniquely restricted to thermal noise originating from the object under examination.

How does it happen that the sample contributes noise to the measured signal? The principle can be understood in a fairly simple way: The human body mainly consists of water, in which different ions like for example Na^+, K^+ or Ca^{2+} are dissolved. These ions are thermally agitated and move. This motion is responsible for a fluctuating current density which is accompanied by an electromagnetic field. The resulting electric field generates a fluctuating voltage across the terminals of the receiver electronics, and is considered as noise.

This noise, in a basic situation, has been described quantitatively by Johnson in 1928 already [77]. Basic theoretical work considering AC-currents has

elucidated the basic principle in the same year by Nyquist in [116]. More suitable for NMR reception is, for example, the theoretical description as presented in the section *A conducting sample* in Appendix A in a publication by Hoult [67]. The derivation is based on the Langevin equation and the law of equipartition of energy from statistical mechanics leading to the following result for the noise squared $< \eta^2 >$:

$$< \eta^2 >= 4k_B T B_W R, \tag{1.17}$$

where T is the temperature of the measured object, B_W the bandwidth of the receiver, and R is the resistance of the measured object seen from the terminals of the receiver electronics. This resistance expresses a principle of reciprocity: The effect of moving ions in the sample onto the noise in the received signal is analyzed by considering the resistance of the sample to a current flowing in the circuit of the receiver!

The macroscopic resistance of the measured object can be calculated with the help of Ohm's law: Because of Ohm's law, the resistance R is equivalent to the power P deposited in the body per unit current in the receiver coil ($U = RI \Rightarrow R = P/I^2$). The dissipated power can be calculated also on a local scale, where Ohm's law states that the current density $\vec{j}$ generated by an electric field $\vec{E}$ depends on the electric conductivity σ: $\vec{j} = \sigma\vec{E}$. The electric field caused by the current in the receiver has two effects: On the one hand, it is responsible for local currents flowing with the velocity $\vec{v} = \vec{j}/\rho = \sigma\vec{E}/\rho$, where ρ is the electric charge density. On the other hand, the field exerts a Lorentz force $\vec{f} = \rho\vec{E}$ onto the moving particles. This force acts on the local currents and performs the work $a = \vec{f}\cdot\vec{v} = \rho\vec{E}\cdot\vec{E}\sigma/\rho = \sigma\vec{E}^2$. By considering that this work is dissipated the resistance can be calculated by integrating over the volume V of the measured object:

$$\begin{aligned} R = \frac{P}{I^2} &= \int_V \sigma(\vec{x})|\vec{E}(\vec{x})|^2\,\mathrm{d}\vec{x} \Big/ I^2 = \int_V \sigma(\vec{x})|E(\vec{x})/I|^2\,\mathrm{d}\vec{x} \\ &= \int_V \sigma(\vec{x})|\vec{\mathcal{E}}(\vec{x})|^2\,\mathrm{d}\vec{x}, \end{aligned} \tag{1.18}$$

where $\vec{\mathcal{E}}$ is the electric field $\vec{E}$ per unit current, denoted as *electric sensitivity* of the receiver coil in this thesis. Note that in the derivation of the latter equation, it has been disregarded that, in MRI, the electromagnetic quantities are high-frequency RF signals. Nevertheless, the latter equation is

still valid (see e.g. Eq. 3 in [200]) with the electric sensitivity $\vec{\mathcal{E}}$ being a complex-valued quantity (just as the magnetic sensitivity $\vec{\mathfrak{B}}$).

The signal-to-noise ratio of the acquired signal can then, within the limits of the used model, be expressed with the electromagnetic properties of the receiver coil and the measured object by combining Eqs. 1.7, 1.15, 1.16, 1.17, 1.18:

$$\begin{aligned} SNR &= \frac{|s|}{\sqrt{(<\eta^2>)}} = C \cdot \frac{|\int_V n(\vec{x})(\mathfrak{B}_x^{re}(\vec{x}) - \mathrm{i}\mathfrak{B}_y^{re}(\vec{x}))\,\mathrm{d}\vec{x}|}{\sqrt{\int_V \sigma(\vec{x})|\vec{\mathcal{E}}(\vec{x})|^2\,\mathrm{d}\vec{x}}}, \\ \text{with} \quad C &= \frac{1}{8}\frac{\hbar^2\gamma^3|\sin(\alpha)|}{(k_B T)^{3/2}}\frac{B_0^2}{B_W^{1/2}}. \end{aligned} \tag{1.19}$$

1.2 Magnetic Resonance Imaging

With the main magnet and the RF-transmit/receive system, a signal is obtained which has information about the whole object. However, according to Eq. 1.15, all locations are encoded nearly equivalently. Therefore signal localization is not achieved with these hardware components; it cannot be differentiated whether the signal originates from one location or another. In MR imaging, the bulk part of spatial encoding is obtained by an additional hardware component: the gradients.

1.2.1 The Gradients

The purpose of the three gradients is to encode information about the locations of the individual signal sources. This task is traditionally solved by generating three spatial magnetic encoding fields (SEMs), whose B_z-components vary linearly along the three different axes of the magnet. An important result of this section is that it is possible to apply these linear SEMs such that the signal data and the spatial distribution of the excited magnetization form a simple Fourier pair. Such a strategy is often used by imaging sequences like the gradient echo or the spin echo, which differ from each other in the way how signal relaxation is exploited to produce a different image contrast (also cf. section 1.2.4, page 33f).

The involved electronics is schematically depicted in Fig. 1.5. The wire windings of gradient coils are typically supported by a cylindrical structure. This geometry is advantageous for hardware integration and especially useful in handling patient scans. The basic gradient coil design, along with one more realistic fingerprint design of an x-gradient coil, is depicted in Fig. 1.6. For practical designs, the wire windings are optimized to compromise between gradient linearity, efficiency, minimal B_x and B_y field strength (=concomitant fields), inductivity, power dissipation and other important coil characteristics.

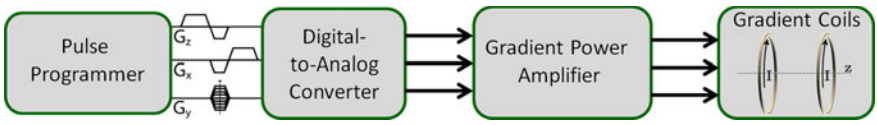

Figure 1.5: Typical gradient driving electronics. The sequence programmer defines the trapezoidal pulse shapes for each gradient channel. The digital instructions are converted to an analog voltage level using a digital-to-analog converter. This voltage is amplified with gradient power amplifiers and finally sent to the gradient coils. The coils generate the linear encoding fields with magnetic field time-courses according to the programmed pulse shapes.

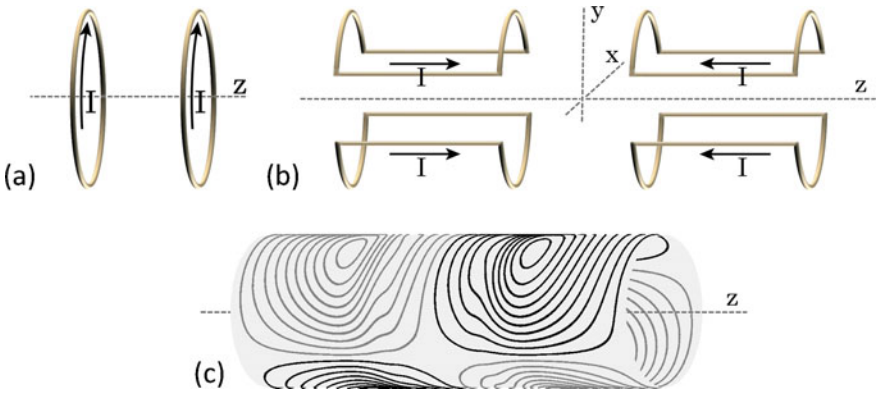

Figure 1.6: Simple and more practical gradient coil wire designs. (a) The basic z-gradient is a Maxwell pair. (b) The basic x- and y-gradients are double-saddle coils (= Golay coils). (c) Fingerprint design of a linear x-gradient coil. The pattern has been optimized using a stream function method with high order smoothness (see chapter 4 in [76]). The image shown is courtesy of Dr. Feng Jia and corresponds to Fig. 4.15a in [76].

1.2.2 Gradient Encoding: Signal Equation for a Single Receiver Coil

The physical principle, which eventually makes localization possible, is simple: The additional linear gradient field changes the precession frequency of the spins along the direction of the field gradient. The received signal therefore has a broadened frequency distribution with a one-to-one correspondence between frequency and location along the direction of the field gradient. With three orthogonal gradients, it is therefore possible to extract the spin density at each location in a unique way. The physical relation between gradient encoding and localization is sketched in Fig. 1.7.

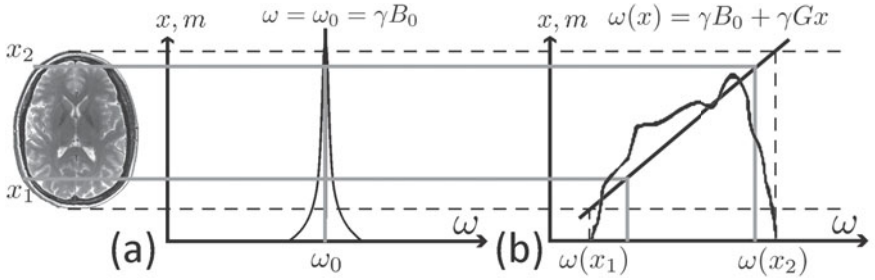

Figure 1.7: The principle of gradient encoding. (a) Without a gradient the magnetic field is constant over the entire object. Therefore the magnetization precesses at the same frequency in the whole object and the frequency content of the signal is represented by a very narrow peak. There is a finite line width in reality because of chemical shift, susceptibility effects and T_2^*-relaxation, among others (the line width shown is vastly exaggerated for reasons of illustration). (b) With a linear gradient field applied along one axis, magnetization vectors perpendicular to that axis still precess with the same frequency. However, along the gradient axis the Larmor frequency is different for each location. This results in a broadened frequency distribution with a one-to-one-correspondence to the spatial coordinate of the signal source.

A rigorous derivation of this result may begin with the dynamics of the magnetization in the fixed frame system, mathematically described by Eq. 1.5. The effective encoding field $\vec{B}_{enc}$, resulting from the superposition of the applied gradient fields, disturbs the main magnetic field. The fields vary slowly in comparison to the precessional motion. The gradient field dynamics can therefore be treated as being static in the equation of motion, given by Eq. 1.5. The resulting motion is a precessional motion with a

frequency corresponding to the magnitude of the overall external magnetic field:

$$\begin{aligned}\omega &= -\gamma \left| B_0 \vec{e}z + \vec{B}_{enc} \right| = \omega_L + (-\gamma B^z_{enc}) + (-\gamma B_\perp)\mathcal{O}\left(\frac{B_\perp}{B_0}\right) \\ &\approx \omega_L + (-\gamma B^z_{enc}).\end{aligned} \tag{1.20}$$

For a scanner with a B_0 on the order of $1 - 3\,\mathrm{T}$, the gradient field B^z_{enc} is typically below $10\,\mathrm{mT}$. The magnitude of the concomitant fields $B_\perp = [(B^x_{enc})^2 + (B^y_{enc})^2]^{1/2}$ is of the same order as B^z_{enc}; in the region of interest (ROI), it is most often even below B^z_{enc}. As a consequence of the large difference between gradient field strengths and main magnetic field strength, the approximation of Eq. 1.20 is very good. Therefore, only the z-components of the gradient fields have a significant impact on the precession frequency of the magnetization vector and the direction of the precessional motion is almost not affected by the gradient fields.

With gradient encoding, the precession frequency of the magnetization (cf. Eq. 1.12) gets a spatial dependency that deviates from the Larmor frequency ω_L in most parts of the object. After the quadrature receiver the complex signal is then modulated with a time and space dependent phase factor $\phi(\vec{x}, t)$:

$$s(t) = \int_V m(\vec{x}) c(\vec{x}) e^{-\mathrm{i}\phi(\vec{x},t)}\,\mathrm{d}\vec{x}. \tag{1.21}$$

This phase factor can be manipulated by the gradient fields in two different ways: application of a gradient field *during* signal readout or *before*. Reconsider Fig. 1.7b. There, it is shown that the application of a SEM *during* signal readout alters the frequency content of the signal. Therefore, this strategy is denoted as *frequency encoding*. The frequency content is different only for spins experiencing a different field strength - therefore localization with pure frequency encoding is only feasible along one spatial direction. Several signal readouts, each encoded with a different gradient direction, could be used to complete signal localization. However, it is also possible to combine frequency encoding with a strategy, where SEMs are applied *before* signal readout. These SEMs do not affect the frequency content of the received signals directly, but spins at different locations acquire a different phase during the application of the SEMs and this phase information modulates the signal when being read out. In this thesis, the term *phase encoding* is used to describe such an encoding strategy.[5]

[5] Note that this definition is broader than often encountered in the MR literature.

Based on Eq. 1.13, it can be shown that, when both strategies are combined, the phase factor in Eq. 1.21 consists of an initial phase from phase encoding and a time-dependent part resulting from frequency encoding:

$$\phi(\vec{x}, t; r) = \phi(\vec{x}, 0; r) + \gamma \int_{\tilde{t}=0}^{t} B^z_{enc}(\vec{x}, \tilde{t}; r)\, \mathrm{d}\tilde{t}. \tag{1.22}$$

The index r has been added because typically (apart from single-shot imaging) a number of signal readouts ($r = 1, \ldots, N_{pe}$) are acquired. The magnetic gradient encoding field $B^z_{enc}(\vec{x})$ is a superposition of the three linear gradient fields $B^z_j(\vec{x})$:

$$B^z_{enc}(\vec{x}, \tilde{t}; r) = \sum_{j=1}^{3} B^z_j(\vec{x}, \tilde{t}; r) = \sum_{j=1}^{3} G_j(\tilde{t}; r) x_j = \vec{G}(\tilde{t}; r)\vec{x}. \tag{1.23}$$

The introduced parameters $G_j, j = 1, 2, 3$, are the *gradient strengths* of the corresponding gradient field.

The latter equation shows that the effective encoding field decomposes into a spatial and a temporal component. The spatial component is predefined by the geometries of the gradient fields.[6] However, the temporal component can be influenced freely by defining the time-courses of the gradient pulse shapes. These temporal degrees of freedom are captured by the introduction of k-space. With the k-space notation the phase distribution of Eq. 1.22 reads:

$$\phi(\vec{x}, t; r) = \left(\vec{k}_r + \vec{k}(t; r)\right) \vec{x}, \tag{1.24}$$

where the initial k-space position $\vec{k}_r$ and the k-space traversal during readout $\vec{k}(t; r)$ are defined as:[7]

$$\vec{k}_r := \gamma \int_{\tilde{t}=0}^{\tau} \vec{G}(\tilde{t}; r)\, \mathrm{d}\tilde{t} \quad \text{and} \quad \vec{k}(t; r) := \gamma \int_{\tilde{t}=0}^{t} \vec{G}(\tilde{t}; r)\, \mathrm{d}\tilde{t}. \tag{1.25}$$

[6] This is where PatLoc imaging becomes interesting: The generalization to arbitrary field geometries introduces new spatial degrees of freedom for MRI signal encoding (cf. chapter 4, page 135ff).

[7] In the literature, it is also not uncommon to define k-space slightly differently with γ replaced by $(\gamma/2\pi)$, see for example [7, 12, 125]. Depending on which definition is used, the factor 2π may, or may not, occur in other equations related to k-space.

In this definition, it was assumed w. l. o. g. that the duration of phase encoding τ is the same for each readout r. Introducing the k-space notation (Eqs. 1.24, 1.25) into the signal equation (Eq. 1.21) leads to:

$$s(t;r) = \int_V m(\vec{x})c(\vec{x})e^{-\mathrm{i}\left(\vec{k}_r+\vec{k}(t;r)\right)\vec{x}}\,\mathrm{d}\vec{x}. \tag{1.26}$$

In the general case, the temporal dimension of the sampling trajectory is important. For example, image contrast, caused by relaxation, is determined by the timing of data sampling. However, in the latter equation explicit time-dependent effects like relaxation have been ignored to focus on spatial encoding rather than temporal effects. Under these assumptions, the signal does not change if the k-space trajectory is traversed differently as long as the set $\mathcal{K} = \{\vec{k}_r + \vec{k}(t;r); t \in [0;T], r = 1,\ldots,N_{pe}\}$ of acquired k-space locations remains the same. Thus, it is possible to eliminate the temporal dependency from the signal equation and Eq. 1.26 adopts a simpler form by only considering the signal values at the sampled k-space location $\vec{k} \in \mathcal{K}$:

$$s(\vec{k}) = \int_V m(\vec{x})c(\vec{x})e^{-\mathrm{i}\vec{k}\vec{x}}\,\mathrm{d}\vec{x}. \tag{1.27}$$

This equation is one of the most important equations in the field of MRI. It shows that signal and spin density, modulated by the RF-coil sensitivity have a Fourier relation. There is only one caveat: The set of sampled k-space locations $\mathcal{K}$ is only a one-dimensional trajectory of finite length within the d-dimensional full k-space $K = \mathbb{R}^d$ required for a true Fourier relation. In chapter 2.2.1c it is shown on page 61 that the finite length of the trajectory is closely linked to image resolution. More subtle is the problem that a true d-dimensional ($d = 2, 3$) image is to be reconstructed from a *one*-dimensional trajectory. It turns out that for sufficiently dense sampling, it is possible to treat the one-dimensional trajectory $\mathcal{K}$ as a d-dimensional subset K of $\mathbb{R}^d$. The reason for this surprising result is described in the paragraph "Completeness of k-Space Encoding" on page 64 in the following chapter. In this thesis, the extended subset $K \supset \mathcal{K}$, $K \subset \mathbb{R}^d$ is called *effective k-space coverage*, or simply *effective k-space*, whereas $\mathcal{K}$ is called *sampled k-space (coverage)*. The concepts of k-space trajectory, sampled k-space coverage and effective k-space coverage are illustrated in Fig. 1.8.

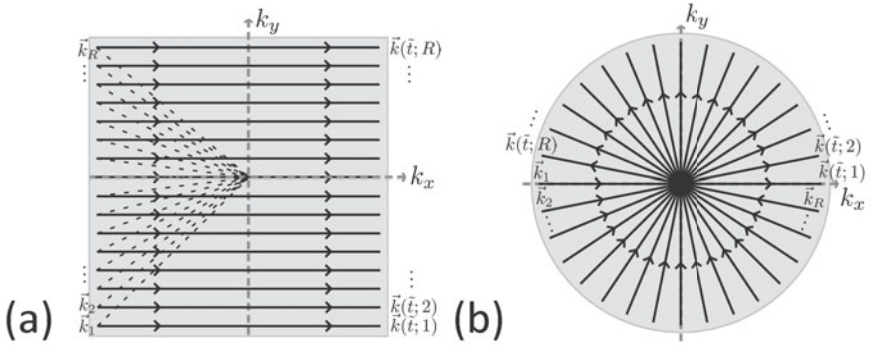

Figure 1.8: k-space trajectory and k-space coverage. (a) Cartesian trajectory. Shown are 16 phase-encodes. The effect of phase encoding, according to how this term is defined in this thesis, is to define the initial k-space position before readout. With the x-gradient, the initial k-space location is shifted along the k_x-axis (often denoted as a *prewinder*) and with the y-gradient along the k_y-axis (phase encoding in the narrow sense). During acquisition, the x-gradient is switched, and k-space is traversed along the corresponding direction. The direction of k-space traversal is indicated by the arrows accompanying the trajectory. When time-dependent effects like signal relaxation are ignored, the direction of k-space traversal can be ignored. The *sampled* k*-space* is given by the black lines. However, the *effective* k*-space* extends around the black lines and is indicated by the gray area. In chapter 2.2.1c it is shown under which conditions this extension occurs. (b) Radial trajectory. By combining x-and y-gradients, the initial k-space positions define locations on a circle in k-space. During readout, the same combination of the gradients, with opposite flow of the coil currents, is used. The trajectory leads to a higher sampling density at the center. A sufficient number of readouts ensures a gap-free effective circular k-space coverage.

For simplicity, consider here complete k-space coverage $K = \mathbb{R}^d$, and a homogeneous RF-coil profile $c(\vec{x}) = 1$ for all $\vec{x} \in V$. Under these special conditions, signal $s(\vec{k})$ and spin density $m(\vec{x})$ form a Fourier transform pair:

$$\begin{aligned} s(\vec{k}) &= \int_V m(\vec{x}) e^{-\mathrm{i}\vec{k}\vec{x}} \,\mathrm{d}\vec{x} = \mathcal{FT}\{m\}(\vec{k}), \\ m(\vec{x}) &= \int_K s(\vec{k}) e^{\mathrm{i}\vec{k}\vec{x}} \,\mathrm{d}\vec{k} = \mathcal{FT}^{-1}\{s\}(\vec{x}). \end{aligned} \tag{1.28}$$

The latter equation mathematically expresses the effect of gradient encoding as the capability to uniquely localize an MRI signal: Under the assumption

of infinitely long sampling, the spin density of the measured object can be retrieved exactly and uniquely at each location. The effect of finite sampling in realistic measurements on the reconstructed images is discussed in the next chapter.

1.2.3 Slice Selection

Without gradients, a large three-dimensional volume $V \subset \mathbb{R}^3$ is excited after application of an on-resonance RF pulse. In many situations, it is useful to excite only thin slices and use two orthogonal gradients for in-plane encoding. This process is called *slice selection* and is achieved by applying a gradient field during transmission of the RF pulse.

Consider a gradient field $B^z_{enc}(\vec{x}) = G_z z$ along the z-axis (= z'-axis) switched during an RF pulse $\vec{B_1}(t) = B_1(t)\vec{e}'_x$. According to Eq. 1.10, the motion of the magnetization in the rotating reference frame is given by:

$$\partial_t^{rot}\vec{M} = \vec{M} \times \gamma(B_1(t)\vec{e}'_x + G_z z\vec{e}'_z). \tag{1.29}$$

In general, a closed-form solution to this equation does not exist and must be found numerically [26, 129]. Under the *small-tip-angle assumption*[8] $M_z(t) = M_z(0) = const$ a closed-form solution exists, revealing insight into the relationship between excited magnetization and pulse shape. With the initial condition $\vec{M}(0) = M_z^0\vec{e}'_z$, in Eq. 1.29 only the transverse components of the magnetization need to be considered further. For symmetric pulse envelopes $B_1(t)$ of duration τ_p, the complex-valued solution $M_\perp = M_x + \mathrm{i}M_y$ to Eq. 1.29 right after the pulse is found to be:

$$M_\perp(\tau_p, \vec{x}) = \mathrm{i}\gamma M_z^0(\vec{x})e^{-\mathrm{i}\gamma G_z z\tau_p/2}\mathcal{F}\mathcal{T}^{-1}\{B_1\}(\gamma G_z z). \tag{1.30}$$

The main result from this equation is that slice profile and pulse envelope form a Fourier transform pair - under the small-tip-angle assumption. In theory, this assumption seems to be good only for flip angles below $20\,^\circ$; notwithstanding, the above Fourier relation is in practice often acceptable for flip angles up to $90\,^\circ$ [96]. An approximately rectangular-shaped slice of thickness Δz is therefore excited with an apodized pulse envelope mimicking a sinc-function of frequency $f = \gamma/2G_z\Delta z$. This result is depicted in Fig.

[8] described for example in chapter 5.1.3.2 of [96].

1.9. When slice selection is performed, it is useful to reduce the signal equation (Eq. 1.28) to a two-dimensional (2D) problem with $\vec{x} \in V \subset \mathbb{R}^2, \vec{k} \in \mathbb{R}^2$ and $\bar{m}(x,y) = \int_z m(x,y,z)\mathrm{d}z$. When the bar over $\bar{m}$ is ignored 2D and 3D imaging problems can be handled with the same notation.

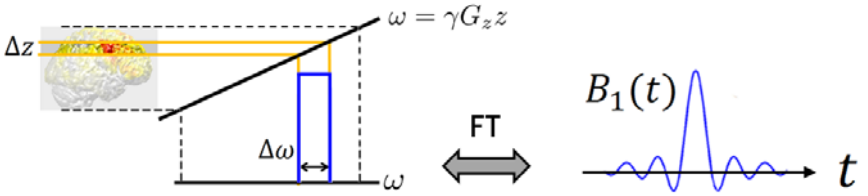

Figure 1.9: Relationship of slice profile and pulse shape. Under the small-tip-angle assumption and linear gradient fields employed, slice profile and pulse envelope form a Fourier transform pair. Note that the Fourier relation is not valid for high flip angles. In this case, no analytic solution to the Bloch equations exists and therefore numerical methods must be used to establish the exact relationship between pulse shape and slice profile.

1.2.4 Basic Imaging Sequences

An important part of MRI research is devoted to the development of various imaging sequences; i.e., the definition of RF and gradient pulse shapes and the timing of signal reception. In the context of this thesis, only two of the most basic imaging sequences are considered: the *gradient echo* [53] and the *spin echo* [56, 59]. Extensive information regarding sequence design is found in the textbook of Bernstein et al. [10].

a) Gradient Echo

The (two-dimensional) gradient echo is a very simple imaging sequence. With Cartesian sampling, k-space is traversed as depicted in Fig. 1.8a. The corresponding pulse sequence is presented in Fig. 1.10a: After slice selection, a phase encoding step brings the k-space vector to the desired position. From this position a line in k-space is read out with a gradient of a fixed amplitude. In contrast to single-shot imaging, an RF-transmit pulse is played out for each acquired k-space line with the repetition time T_R. This ensures reduced signal dephasing, which is due to magnetic field inhomogeneities, mainly caused by susceptibility differences, which have

been ignored in the signal equation (cf. Eq. 1.27). For long echo times T_E (i.e., the time between RF pulse and center of signal readout) and long T_R, the resulting contrast is often referred to as the T_2^**-contrast*.

b) Spin Echo

An important advantage of a spin echo is that the effect of static magnetic field inhomogeneities is eliminated. Whenever magnetic field inhomogeneities would deteriorate the image quality, a spin echo will produce superior image quality. The imaging sequence is depicted in Fig. 1.10b. In contrast to a gradient echo, two RF pulses are played out prior to data acquisition. The effect of the second pulse is to reverse the signal dephasing taken place since the application of the first pulse. Repetition time T_R and echo time T_E (i.e., the time between the first RF pulse and the center of signal readout) are chosen according to the desired imaging contrast. For long T_E and long T_R the contrast is often referred to as the T_2*-contrast*.

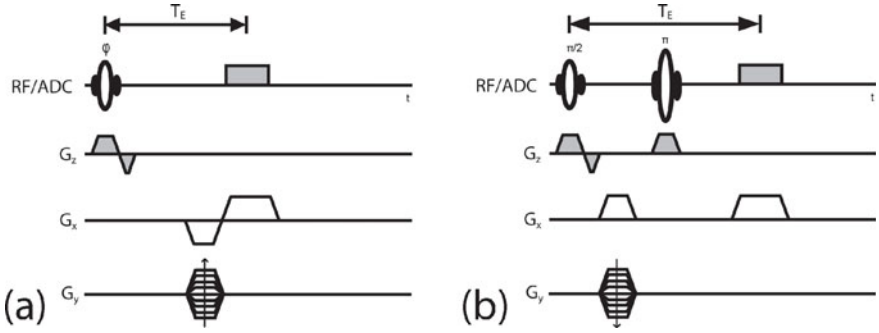

Figure 1.10: Two basic imaging sequences. (a) Gradient echo. (b) Spin echo.

1.3 Parallel Imaging[9]

In the early years, only a single RF coil was used for MRI measurements. From about 1990 on, initial experiments were performed with multi-coil receiver arrays. Initially, such arrays were used to improve SNR [145]. The potential of multi-coil arrays to accelerate MR image sequences [173, 135] was recognized only in the late 1990s and since then research in the field of parallel imaging has exploded. In this section, imaging with an RF array is introduced, some of the most important implications of parallel imaging to MRI are briefly discussed and the signal equation for multi-coil acquisitions is presented.

1.3.1 RF-Receiver Array

Before the advent of multi-coil RF arrays, MRI scanners were typically equipped with one large RF-volume coil. Such a volume coil is typically designed to have a homogeneous sensitivity. This is beneficial because then the coil is equally sensitive to all parts of a measured object. In contrast to such homogeneous large volume coils, small RF coils, placed near the surface of the object under examination, are not sensitive to the whole object. Nevertheless, Roemer et al. realized in 1990 that such surface coils can be useful in MRI when several of those surface coils are combined to an array of coils surrounding the measured object (cf. Fig. 1.11a). Even though the individual elements are only sensitive to a limited region of the imaging volume (cf. Fig. 1.11b), the combination of all coils is sensitive to the whole volume with a tendency of a higher sensitivity near the surface of the object, and for field strengths above about 1 T for human systems a high sensitivity can also be observed at the center; this phenomenon is sometimes termed *dielectric resonance* (see for example the root-sum-of-squares[10] sensitivity image in Fig. 1.11c). Fortunately, the sensitivity variations have proven to be rather unproblematic in practice.

[9] In this thesis, the term *parallel imaging (PI)* is used in a broad sense. Sometimes, PI is used in a narrower sense comparable to the term *partially parallel imaging (PPI)*, typically used to denote accelerated imaging with the help of an RF array. Here, however, PI refers to all imaging experiments where data are acquired with several RF coils. PI is therefore defined here as *multi-coil imaging* opposed to *single-coil imaging*.

[10] The root-sum-of-squares involves: (a) multiplication of each voxel value with its complex-conjugate and (b) formation of a single image from the several coil images by summing up the (squared) voxel values and (c) taking the square root of the formed single image.

Figure 1.11: RF-receiver coil array with sensitivity maps. (a) Twelve-channel head receiver coil array for a MAGNETOM Trio, A Tim System 3T, Siemens Healthcare, Erlangen, Germany. (b) Four RF-coil sensitivity maps at $3\,\mathrm{T}$ of the coil shown in (a), where each map has been combined from three others. The maps were determined by dividing images of each receiver channel, acquired with a homogeneous phantom, by the corresponding RF-transmit field maps, which were measured similar to the method described in [34]. (c) Root-sum-of-squares image of the RF-sensitivity profiles.

It is an important feature of a receiver array that it consists of several coils, each of which generating a separate signal - in parallel. Each signal channel should provide as much independent information as possible. Thus, it is important that the individual coils are not strongly coupled to each other. RF-coil decoupling strategies (see e.g. chapter 3.4.2 in [90]) are therefore of great interest to the RF engineer with important consequences for the optimal coil geometries. At the same time, the coils should be placed as near as possible to the measured object in order to enhance the SNR. These and other concerns explain why modern whole-body MR scanners are often equipped with a multitude of different RF-receiver arrays, where each array is optimized for a different medical application. For example, there are cardiac, spine or knee arrays. Another example is Fig. 1.11a, where a head coil array is shown.

1.3.2 Implications of Parallel Imaging

Signal reception with several coils has the advantage over single-coil measurements that each RF coil is sensitive in different object regions; thus, an RF-receiver array provides spatial information in addition to gradient encoding. And this additional information is not generated sequentially as done with gradients, but in parallel; i.e., at the same time. Therefore, the information gained with an array almost comes “for free”. The additional information can be used in various ways. Some of the most important implications to MRI are presented here.

a) Increased SNR

In 1990, Roemer et. al presented in their seminal publication [145] that parallel acquisition can significantly enhance the SNR of the reconstructed images. The basic idea relies on an optimal combination of the different coil images. An adequate optimization can be formulated as a reconstruction problem and is therefore discussed in more detail in the next chapter, see in particular the *Remark* on page 78.

b) Acceleration of MR Measurements

Even more important is that PI can be used to significantly accelerate MRI scans. The duration of patient examination is not only a question of sufficient resources or patient comfort. Among others, shorter measurements significantly reduce motion artifacts. For single-shot techniques, such as EPI [109] (also cf. chapter 3.4.2 in [212]), it is advantageous to shorten measurements in order to reduce susceptibility artifacts. Also functional MRI [113] profits from a higher temporal resolution such that even 3D single-shot acquisitions become feasible.[11] The usage of PI in this context has already been suggested in the late 1980s and early 1990s [18, 70, 82, 88, 139]. Further technological and theoretical developments in the late 1990s [173, 135] leveraged the original ideas to the wide-spread acceptance of PI in research and clinical environments. The role of PI for the acceleration of MR measurements is best understood in the context of image reconstruction and is therefore discussed in chapter 2.3, page 72ff.

c) Further Applications

Further applications of PI are reviewed in [90] including artifact removal caused by coherent k-space inconsistencies and the reduction of motion artifacts. Another interesting application of PI is the fast determination of B_0-inhomogeneities [175, 174]. In the context of parallel imaging, the presented PatLoc imaging concept can also be regarded as a further interesting application of PI.

[11] A modern example of an ultra-fast 3D trajectory is found in [211].

1.3.3 Signal Equation for Several Receiver Coils

When several receiver coils are considered in an RF array, cross-talk between the coils can occur. With modern decoupling techniques, this cross-talk is often reduced to a negligible level in high-quality receiver arrays and the received signals behave nearly independently from each other. Therefore, the signal equation derived for the single-channel case in Eq. 1.27 is valid also in multi-coil arrangements. An array with N_c signal channels then generates separate signals $s_\alpha(\vec{k})$:

$$s_\alpha(\vec{k}_\kappa) = \int_V m(\vec{x}) c_\alpha(\vec{x}) e^{-\mathrm{i}\vec{k}_\kappa \vec{x}} \,\mathrm{d}\vec{x} \quad \text{for all} \quad \alpha = 1, \ldots, N_c. \tag{1.31}$$

The index κ has been introduced to indicate that only a finite number of data points at $\vec{k} = \vec{k}_\kappa$ are stored for post-processing. The difference between the individual signals results from the different spatial distributions $c_\alpha(\vec{x})$ of the RF-coil sensitivities. Note that, even when the individual channels cannot be regarded as being completely decoupled, the above equation is still valid. If needed, the RF-coil sensitivities are measured in a separate scan using the same hardware configuration. Therefore the cross-talk is implicitly accounted for when the sensitivities are extracted from the data. A detailed analysis of the effects that coupled RF coils have on MRI signals and reconstructed images is found in [118], chapter 3, page 73ff.